Monolithic high peak-power coherent Doppler lidar system

Leonid V. Kotov*[a,b], Albert Töws[c], Alfred Kurtz[c], Konstantin K. Bobkov[a], Svetlana S. Aleshkina[a], Mikhail M. Bubnov[a], Denis S. Lipatov[d,e], Alexey N. Guryanov[d] and Mikhail Likhachev[a]
[a]Fiber Optics Research Center RAS, 38 Vavilov Street, 119333, Moscow, Russia
[b]Moscow Institute of Physics and Technology, 9 Institutskii per., 141700, Dolgoprudny , Russia
[c]Cologne University of Applied Science, Steinmüllerallee 1, 51643, Gummersbach, Germany
[d]Institute of Chemistry of High Purity Substances RAS, 49 Tropinin Street, 603950, Nizhny Novgorod, Russia
[e]Lobachevsky State University of Nizhny Novgorod, 23 Prospekt Gagarina, 603950, Nizhny Novgorod, Russia

ABSTRACT

In this work we present a monolithic lidar system, based on a newly-developed double-clad large mode area (LMA) polarization-maintaining Er-doped fiber and specially designed LMA passive components. Optimization of the fiber designs resulted in as high as 100 W of SBS limited peak power. The amplifier and its passive components (circulator and collimator) were integrated in an existing lidar system. The enhanced lidar system provides three times increase of scanning range compared to one based on standard telecom-grade amplifiers.

Keywords: fiber amplifiers, single-frequency amplifiers, coherent Doppler lidar, Er-doped fibers

1. INTRODUCTION

Coherent Doppler lidar is a key technology for remote atmospheric wind speed measurements. Using Er-doped fiber (EDF) amplifiers in master oscillator power amplifier (MOPA) configuration at 1.55 μm in all-fiber coherent Doppler lidar systems has become more attractive due to many advantages in terms of eye safety, stability, availability of optical components, maintenance, and compactness. Sources with linewidth of tens of kHz (to keep the coherence between the seed and backward scattered over the 10 km scanning range) and pulse duration of hundreds of nanoseconds (to keep resolution below hundred of meters) are required for this system. In such a condition the stimulated Brillouin scattering (SBS) is the main factor that limits peak power of the pulse utilized in the lidar system and in this way - the maximum scanning range. As a result, peak power of standard telecom-grade fiber amplifiers is SBS limited at value of ~10 W, which does not allow one to increase scanning distance to be more than 1-2 km [1,2]. Standard technique to suppress SBS is increasing mode field diameter (MFD) of the fiber and shortening its length [3-6], resulting in typical peak-power for such systems of hundreds of Watts. Recently record peak-power of 4 kW was demonstrated by our group from single-frequency Er-doped amplifier based on just 1 m of active fiber with 500 μm^2 mode area [5]. At the same time presence of passive optical components at the amplifier output in monolithic lidar configuration and requirement of stable long-term operation out of laboratory environment lead to significant decrease of available peak-power. Moreover, the ability to maintain polarization is a natural demand of the most sensitive wind lidar systems [1]. In this work we present a high peak-power monolithic lidar system design optimization and show the amplifier characteristics for different wavelengths. Finally, we demonstrate its application for wind speed measurements.

*kotov@fo.gpi.ru; phone +7 499 135 74 02; fax +74991358139; fibopt.ru

Fiber Lasers XIII: Technology, Systems, and Applications, edited by John Ballato, Proc. of SPIE
Vol. 9728, 97282U · © 2015 SPIE · CCC code: 0277-786X/15/$18 · doi: 10.1117/12.2213165

2. FOUR-WAVELENGTH DOPPLER-LIDAR WITH PULSE SHAPE CONTROL

2.1 Lidar system setup

The system setup of the four-wavelength Doppler lidar with a feedback controlled pulse shaping unit is shown in Figure 1.1. The four-wavelength lidar mainly consists of five sub-assemblies: Master oscillator unit (MOU), pulse-shape control unit (PSCU), amplifier and transceiver unit (ATU), detector unit (DU), and signal processing unit (SCU). All components of this lidar system are polarization maintaining and fiber-based.

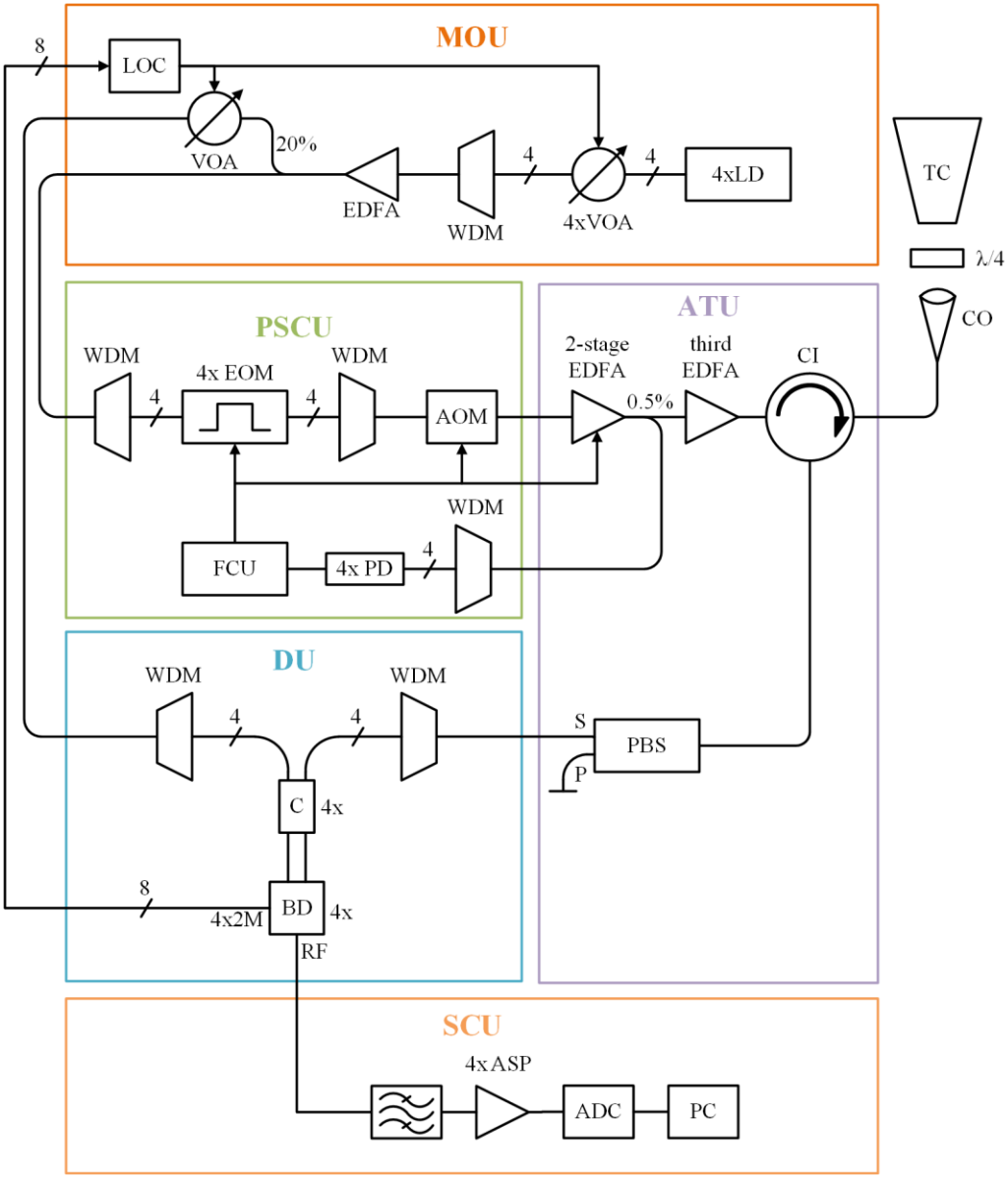

Figure 1.1: Four-wavelength coherent Doppler-lidar system setup: Master oscillator unit (MOU), pulse-shape control unit (PSCU), amplifier and transceiver unit (ATU), detector unit (DU), and signal chain unit (SCU), external cavity laser diode (ECLD), wavelength division multiplexer (WDM); local oscillator control (LOC); variable optical attenuator (VOA), erbium doped fiber amplifier (EDFA), electro-optical modulator (EOM), acousto-optical modulator (AOM), feedback control unit (FCU), photo diode (PD), circulator (CI), collimator (CO), telescope (TC),– coupler (C), polarization beam splitter (PBC), balanced detector (BD), analog signal processing (ASP), analog to digital converter (ADC).

The master oscillator unit (MOU) consists of four external cavity diode lasers. Every laser wavelength is separately generated and tuned. The wavelengths are chosen from the ITU-grid (IUT: International Telecommunication Union) near 1.55 µm for best transmission through the atmosphere. The chosen wavelength-channels are channel 27, 31, 34, and 36. The intensity of those wavelength-channels is different due to the tuning process, because changes in temperature and current influence the output intensity of those diode modules. Therefore, electronically changeable variable attenuators (VOA) are used to compensate those changes in intensity. The VOAs are feedback controlled by the local oscillator control unit (LOC). The intensity of the local oscillator of every channel is measured using the monitor outputs of the balanced detectors (BD).

All four channels are multiplexed by a wavelength division multiplexer (WDM) and amplified by one EDFA to a total power of 200 mW. A part of that laser light is used as the local oscillator. The LOC controls the VOA for an optimum intensity value for optical amplification.

80% of the MOU laser light is directed to the pulse shaping unit, where the laser light is demultiplexed, in order to shape the pulses of each channel with electro-optic modulators (EOM) separately. Then, all pulses are frequency shifted by an acousto-optic modulator (AOM) to measure positive and negative radial wind velocities. The pulses are additionally shaped by this AOM. Using both modulators for pulse shaping, the minimum needed extinction ratio of 70 dB can be achieved.

The shifted and shaped pulses are amplified with a two-stage EDFA. To monitor the pulse shapes, 0.5 % of the output pulse power of the EDFA is used. After attenuation, the wavelength-channels are demultiplexed. Four fast photodiodes measure the shape of the pulses for each wavelength separately. The pulses are digitized with a sampling rate of 100 MHz by an analog-to-digital (ADC) converter within the feedback control unit. This unit controls the EOMs, the AOM, and the second stage of the two-stage EDFA. After pre-amplification the shaped pulses are amplified in the third EDFA stage, which is described in chapter 3 in more detail.

Via a circulator the amplified pulses are directed to the collimator, where the laser pulse is decoupled. The linear p-polarized laser pulse is circular polarized after passing a quarter wave plate. The beam diameter is expanded to 60 mm using a Kepler refractor with aspheric lenses. The backscattered light from the aerosols is transformed into s-polarized light and coupled back into the fiber where the laser pulse is directed to the polarization beam splitter via the circulator. Using this polarization sensitive transceiver, the overall isolation of the sent pulses is increased up to 80 dB, keeping the power below the saturation threshold of the balanced detector.

In the detection unit the wavelengths of the local oscillator and the backscattered light are demultiplexed, thus, every channel can be coupled separately to its balanced detector. The amplified differential signal eliminates the DC and amplifies the AC component of the heterodyne signal. The bandwidth of this heterodyne signal is defined by a bandpass filter and amplified with a low noise amplifier. By means of four ADCs the amplified heterodyne signals are digitized with 1 GS/s (or 500 MS/s) and 8 bit resolution. The raw data are sent to the personal computer (PC) to extract the information about wind velocity and signal strength. For real time data processing the graphical processing unit (GPU) is used.

2.2 Control of different pulse shapes and durations

With respect to Figure 1.1, the control circuit uses 0.5% of the output power to measure the power and the shape of the EDFA amplified output pulses. The wavelength-channels are demultiplexed after attenuation. Four fast photodiodes measure the shape of the pulses for each wavelength separately. The pulses are digitized with 100 MHz. For a larger control range it is useful to preshape the pulses with the AOM. The feedback control unit calculates a corrected seed pulse shape for each channel which is applied to the EOMs.

The calculation is based on two nested control loops: The EOM controller loop which controls the EOM values for the pulse shaping unit and the EDFA controller loop which regulates the pump power of the EDFA. The EOM controller regulates each sampled point, starting from the beginning of the pulse. The EDFA controller sets the amplification depending on the value of all controlled points per pulse. The peak power can be set by the user, however, it is often set to SBS threshold.

Figure 1.2 shows an example of two feedback controlled pre-amplified pulses, which are simultaneously amplified in the two-stage EDFA. As seen the pulse shapes are perfectly shaped and stabilized. The developed feedback controlled pulse shaping unit is capable of adjusting any given pulse shape with a pulse duration from 100 ns to 1200 ns. The only limitation for the sake of stability is the rise-time and falling-edge time of at least 20 ns.

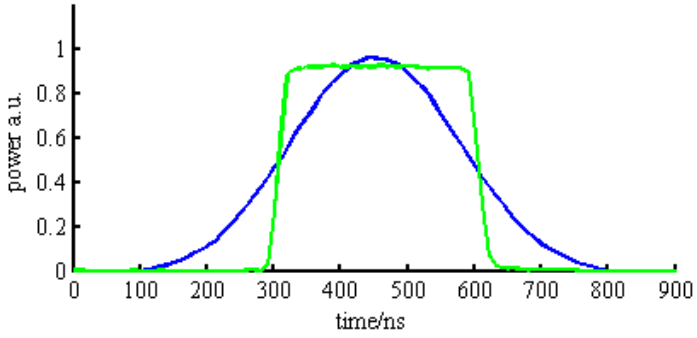

Figure 1.2: A Gaussian and square shaped pulse simultaneously pre-amplified and feedback controlled on two different channels.

By amplifying those pulses with the third EDFA stage, which is described later, the pulses are additionally distorted due to gain saturation. The influence of the gain saturation can be partially compensated, but to guarantee long-term stability, it will be better to include the third EDFA in the feedback circuit and algorithm.

2.3 Signal processing

The lidar can be operated in two signal processing modes: In real time processing, as mentioned above, and in signal store mode. For the atmospheric measurements in chapter 4 the real time processing mode was chosen. The received heterodyne signals for all channels are digitized with 1 GS/s (or 500 MS/s) and 8 bit resolution. The raw data are sent from the capture card directly to the graphical processing unit over PCIe. Further calculation and visualization is done in parallel computing by the graphic card.

The heterodyne signals are divided into range gates. The range gates for all channels are square shaped and equal to the pulse durations for each channel. Each range gate is transformed into the frequency domain using fast Fourier transformation (FFT). If the range gate sampling points do not match 2^n, zero padding is used to fill the data. Because the signal-to-noise ratio is typically very low, the spectra are accumulated to enhance the detectability. To even out the noise floor, every range gate is subtracted by the last or a range gate, which contains no signal.

The detection line is often defined at 5 dB over the standard deviation of the spectral noise. If the signal is over that detection line, the frequency component in the backscattered light is detected. To enhance the precision of peak-frequency estimation, a fit with a quadratic equation is implemented. The peak (vertex) of the resulting fit with the accumulated spectrum is used to determine the radial wind velocity v_r, using the well-known equation for a monostatic Doppler-lidar:

$$v_r = \frac{(f_{peak} - f_{AOM}) \cdot \lambda}{2} \quad ,$$

where f_{peak} is the peak frequency in every range gate, f_{AOM} the frequency offset due to the use of an AOM (110 MHz), and λ the wavelength of the laser output pulse.

3. HIGH-POWER AMPLIFIER

3.1 PM LMA EDF design

The best results in peak power scaling of single-frequency lasers at 1.55 μm were obtained by our group using specially designed LMA Yb-free Er-doped fiber with cladding pumping at 980 nm. The Er-doped fiber design is based on utilization of ternary P_2O_5-Al_2O_3-SiO_2 glass for fabrication of an Er-doped core [7]. This glass matrix (1) has a refractive index similar to that of undoped silica glass. This allows keeping single mode regime at large core diameters. And (2) at the same time, it provides good solubility of erbium clusters – our study have shown possibility to increase Er^{3+} ions content by 1.5 times as compared to standard Al_2O_3-SiO_2 glass with the same refractive index and keep the same pump-

to-signal conversion efficiency. Thus, large mode area fibers with P_2O_5-Al_2O_3-SiO_2 core and high erbium concentration show better performance compared with standard Al_2O_3-SiO_2 counterparts [7].

The P_2O_5-Al_2O_3-SiO_2 Er-doped fiber preform was produced by Modified Chemical Vapor Deposition (MCVD) technique. $SiCl_4$, $POCl_3$, $AlCl_3$, and $Er(thd)_3$ were used as precursors. The uniform Er-doped P_2O_5-Al_2O_3-SiO_2 core was produced by the following procedure. At first, a thin porous layer of P_2O_5-Al_2O_3-SiO_2 glass was deposited. After that, $Er(thd)_3$ vapor together with oxygen were supplied into reaction zone. As a result, forming Er_2O_3 particles were deposited on the porous layer. Then the porous layer was sintered in flowing CCl_4 and in oxygen to remove OH^- groups. Required refraction index profile was obtained due to layer-by-layer core deposition with controllable phosphorous and aluminum concentrations, providing excellent homogeneity of the oxides distribution. It is worth noting, that fully gas phase technology resulted in superior purity of the glass due to high sterility of the process and much cleaner precursors compared to e.g. solution-doping or powder techniques.

The preform cladding was etched to reach required core-to-cladding diameter ratio. Then two borosilicate rods were incorporated into the preform to provide it with polarization maintaining properties. A fiber was drawn down from the preform. The core/cladding diameter of the fiber was 36/130 μm. The fiber was coated with polymer, providing a NA of 0.45 for the pump. The refractive index between core and cladding was ~0.001. An additional F-doped layer (with refractive index below that of silica) was added near the core to provide robust single-mode operation and low bending sensitivity. The fiber could be bent with a diameter of less than 12 cm with no observable loss. Cladding pump absorption was measured to be 2 dB/m at 980 nm.

It should be noted that the birefringence of a PM LMA fiber is lower than that of fiber with normal core and the same stress rods size. The thing is, that stress induced by rods has a high intensity in a rather narrow area at the center of the fiber. So, the overlap of large core and stress profile is quite small. Although larger stress could be obtained due to usage of thicker rods, their diameter is limited by available space between core and cladding dimensions. The increase of outer clad diameter would result in a smaller pump absorption (due to reduction of the core/clad diameter ratio) and longer optimal length of the Er-doped fiber, which is unacceptable due to the lower threshold of nonlinear effects. So, production of LMA PM fiber with satisfactory birefringence became quite challenging. Two versions of the fiber with rod sizes ~20 and 30 μm were manufactured (Figure 3.1). The 5 m length of both fibers show polarization extinction ratio (PER) > 15 dB in passive transmission experiment (a wide-band source centered out of absorption band of Er ions – near 1600 nm was used). However, this value significantly decreases for fiber with smaller rods during high power operation regime due to low birefringence provided by small rods and heat induced stress in the core. So, although production of fibers with 20 μm rods is much simpler from the technological point of view, it turns out that such fibers do not demonstrate acceptable PER while operating at high power. Therefore, a fiber with large rods was used in the following experiments.

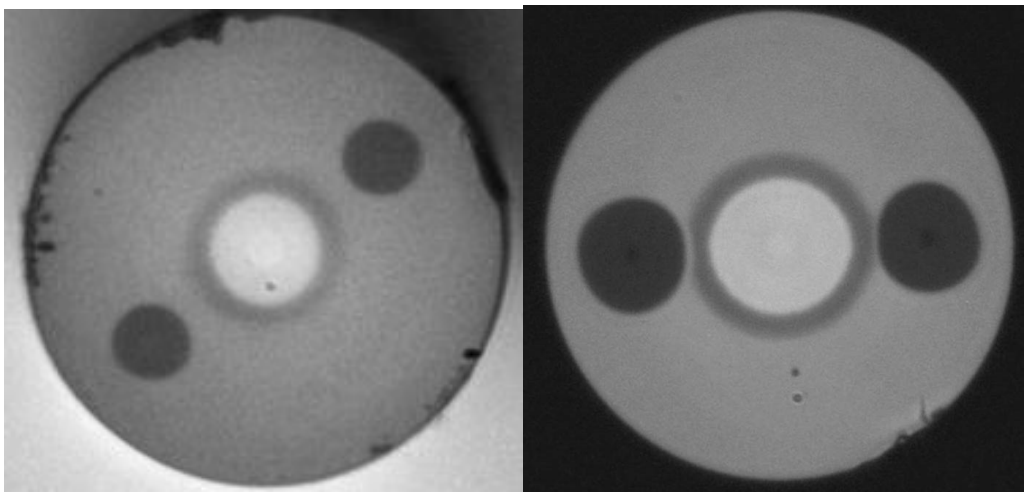

Figure 3.1. Microscope image of fibers with different size of stress rods.

3.2 Passive fiber design

It should be stressed that standard fiber components, based on SMF28 fiber (or its PM analogue), could not be used for high peak power lidar fabrication. There are two reasons for this. First, there is a strong MFD mismatch between LMA Er-doped fiber and standard SMF28 and PM8/125 μm fiber, which results in a high splice loss. Second, and even more important, the SBS threshold is observed at a peak power of only ~50 W for one meter length of standard fiber. As a result, the passive fiber is the factor that limits maximum peak power at the output of a fiber-based lidar system.

To overcome the above mentioned limitations, we have designed a special LMA passive fiber. Most important design criteria were matching the developed LMA Er-doped fiber in terms of MFD, relatively low bend sensitivity, and single-mode operation. Further, a superior ability to maintain polarization is required for the passive fiber – when the passive components are built on the base of such fiber, micro-bending and packaging could strongly deteriorate the output PER and therefore the performance of the whole system. One more demand to the passive fiber is a shift of SBS gain spectra relative to the active fiber (could be achieved by careful control of the core composition) - otherwise the SBS threshold would strongly decrease when passive fiber is added to the output of the system.

A PM LMA fiber with these adjusted requirements was manufactured by our group. The SBS threshold was measured using 100 ns pulsed laser as a function of length for this fiber (Fig. 3.2). As expected the SBS threshold is inversely depends on the passive fiber length. It should be noted, that for 100 ns pulse duration SBS threshold might increases by ~ 1.5-2.5 times as compared to CW radiation (depend on SBS gain spectrum of the fiber), so for a longer pulses one may expect a lower SBS threshold value. In any case it could be seen that with the new passive fiber design the SBS threshold of 1m fiber (typical pigtails length between active fiber and output isolator) shifts from tens-of-W (for SMF28-type fiber) to hundreds-of-W level. Of course, a careful control of net pigtails length is required in this case as it is become a main limiting factor for the high-peak power amplifiers. It is worth noting that for kW-level single frequency lasers at 1.55 μm this passive fiber could not be used and another solution is required to add output elements (tap port for signal control, circulator, collimator, and etc.).

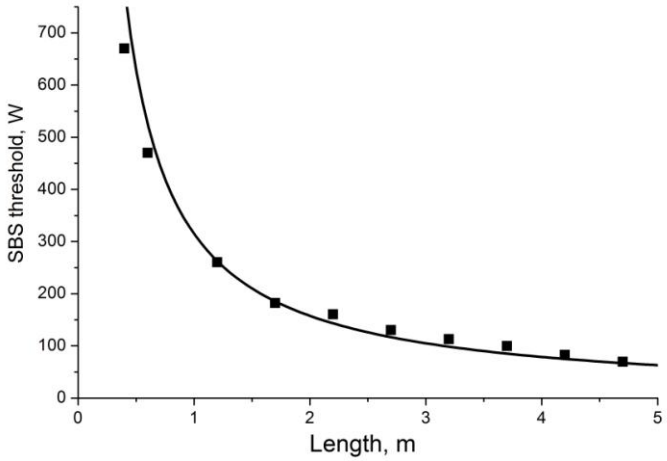

Figure 3.2. SBS threshold of Ge-doped LMA fiber.

3.3 Amplifier scheme

Figure 3.3 represents the principal optical scheme of the high power amplifier unit of the lidar system including booster and passive output components for pulse delivering and scattered light detection. The built unit was terminated with standard FC/APC adapters for seed signal. For amplified signal output and for collecting the backscattered light with a collimator an armored optical cable was used. The input signal in fast polarization axis together with the pump light from multimode diodes at 976 nm were launched into 5 m of polarization maintained (PM) LMA EDF active fiber through (2+1) x 1 pump combiner. Unabsorbed pump power at the end of active fiber was removed by in-house made cladding light stripper (CLS) based on LMA PM passive fiber, described in previous paragraph. A few percents tap coupler was added to control the signal shape. A custom made 3-port PM circulator was spliced between the cladding light stripper and output collimator in order to guide the backscattered signal from the atmosphere towards the detection unit. Only the

fast polarization axis of the circulator was working in forward direction, while radiation in both axes was transmitted from port 2 to port 3. The same LMA PM passive fiber was used in this component. The λ/4 wave plate is typically placed at the output of the amplifier, so the polarization plane of the atmospheric signal is rotated by 90° relatively to the polarization of the amplified pulses. Therefore, the returned-from-atmosphere-signal was launched into the slow polarization axis of the output fiber. A polarization beam splitter (PBS) was spliced to the 3rd port of the circulator in order to separate the collected signal from the atmosphere and a small part of output pulses back-propagating in fast polarization due to reflection on splices and interfaces of components. The isolation of the circulator itself (port 1 to port 3) was ~ 60 dB. At the same time, usage of PBS increased this value to >79 dB. This fact confirms high polarization maintaining properties of the developed passive fiber. The M^2 at the output of collimator was measured to be ~ 1.1, which demonstrates single-mode operation of the developed LMA PM passive fiber.

The overall loss-of-signal (decrease of signal at the collimator output relative to the signal at the output of active fiber) in assembled passive components was found to be ~2.5 dB including components loss (~1.4 dB), splice loss (~0.8 dB), and packaging loss (~0.3 dB). So, the lidar output power is ~1.8 times lower than the power at the output of the amplifier. Also it should be noted that with standard fusion splicer compatible with PM fibers it is quite challenging to splice components having pigtail length less than 15 cm. Therefore, net passive fiber length before circulator exceed 75 cm (30 cm for each of CLS and coupler + 15 cm for one side of circulator). By this reason the maximum peak power of the amplifier was limited by passive components at value less than 400 W before circulator and ~ 300W after collimator (due to loss of signal in circulator and collimator) for 100 ns pulses and even less for a longer pulses.

The amplifier body without pump units was quite compact with 25x17x4 cm footprint. Then amplifier, pumps, cooling, and electronic systems were mounted into a 47.4x30x13.5 cm standard case (Fig. 3.4).

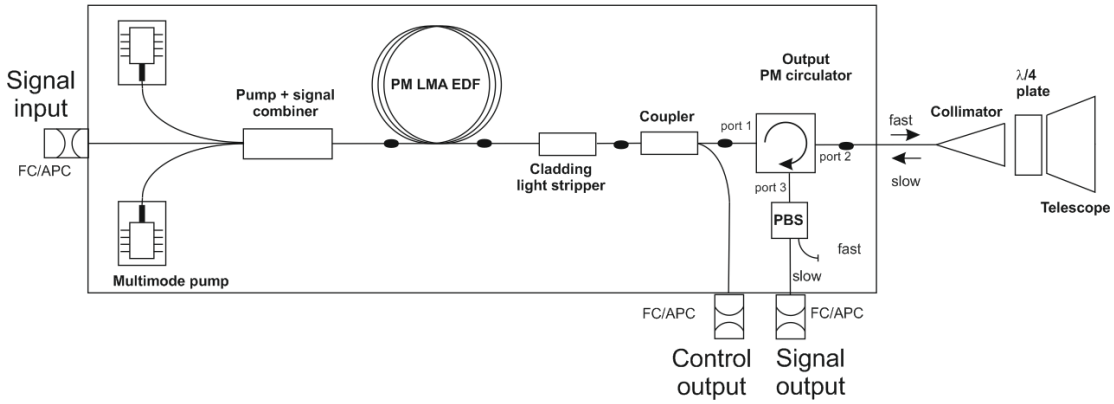

Figure 3.3. High power amplifier unit.

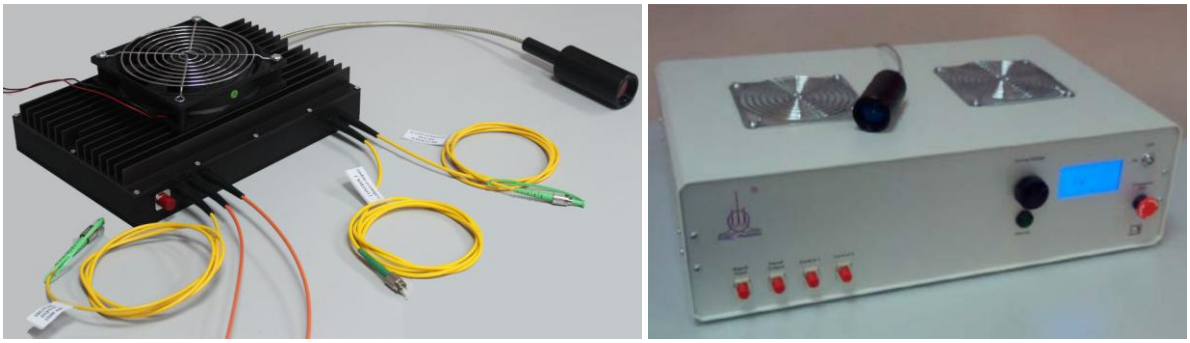

Figure 3.4. Photo of amplifier (25x17x4 cm) (left) and the same units packed into a standard case together with the pump source and electronics (47.4x30x13.5 cm).

3.4 Performance of the lidar system

The erbium concentration of LMA EDF was not optimized, so relatively high length of 5 m was required to absorb all pump power. As a result, the SBS threshold of the amplifier was the limiting factor of the peak power in the presented scheme. As indicated in the previous paragraph the lidar output power (and therefore SBS threshold) is ~1.8 times lower than the amplifier output power. At first, the dependence of the SBS threshold of the lidar system on pulse duration at 10 kHz repetition rate was measured for pulses at different wavelengths (Fig. 3.5). The SBS threshold was defined at the peak power where the instability of the output pulse appeared. The cause of this instability is the generation of the first order SBS Stokes wave [5]. It can be clearly seen that the SBS threshold increases with wavelength. This fact could be associated with the signal distribution along amplifier length. Short wavelength signals have a high gain at the beginning of the EDF. As a consequence, the SBS threshold is reached at lower peak power compared to signal at longer wavelengths. Another found trend, shown in Fig 3.5, is the increase of SBS threshold (by more than two times when pulse duration was switched from 100 ns to 800 ns) with signal pulse duration decrease. This is a result of spectral broadening of shorter pulses. As a result, maximum peak power was limited by a value of 80-100 W for 400-800 ns pulses. For such pulses we estimate threshold in the passive part of lidar to be about 100-150 W as well, so the performance of the all-fiber amplifier could not be improved significantly without of father optimization of the passive components at the output of the amplifier.

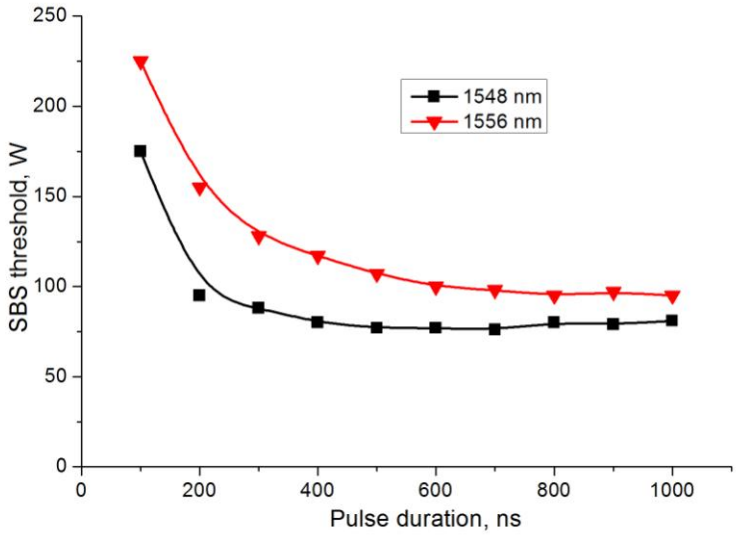

Figure 3.5. SBS threshold dependence on pulse duration for different wavelengths.

Also the dependence of the SBS threshold on pulse repetition rate was measured (Fig. 3.6) for 500 ns duration and 1556 nm wavelength of seed pulses. Although no change in the SBS threshold with repetition frequency was expected, we found growth of the threshold power for frequencies less than ~20 kHz. Though the nature of this effect is not clear at the moment, the same behavior was found for a standard telecom-grade amplifier tested in similar conditions.

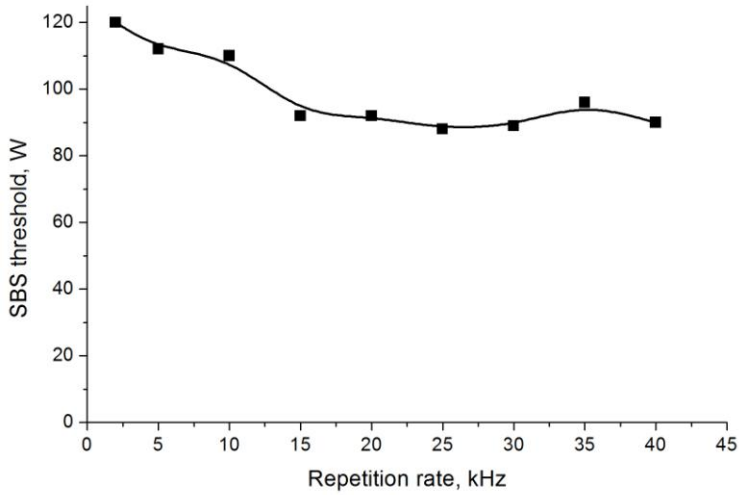

Figure 3.6. SBS threshold dependence on pulse repetition rate.

4. ATMOSPHERIC MEASUREMENTS

In this state of development, the atmospheric real-time measurements are taken from the window in our laboratory in Gummersbach (Germany). To make RHI measurements (RHI: range height indicator), we use a 1D-scanner. An example of such a RHI scan is shown in Figure 4.1. This RHI-scan shows a measurement example taken with the above described third amplifier stage. The peak power was set to SBS threshold at about 100 W, using square shaped pulses. The measurement was taken with a pulse duration of 800 ns, which corresponds to a range resolution of 120 m. The pulse repetition frequency was set at 10 kHz. With 2000 accumulations this results in a time resolution of 0.2 s. The angle resolution was at 1°. Consequently, the measurement needs 24 s for one scan from 30° to 150° elevation angle.

At the top of Figure 4.1 the measured radial wind velocity is displayed, which was about 6 m/s on that day. At the bottom of Figure 4.1 the signal amplitude is shown. The amplitude is color coded in logarithmic scale and range corrected. It is seen that the boundary layer was at 2.2 km and the cloud layer at about 4 km height on that day. Between those layers the received signal was too weak to detect. This is due to the poor particle density above the boundary layer.

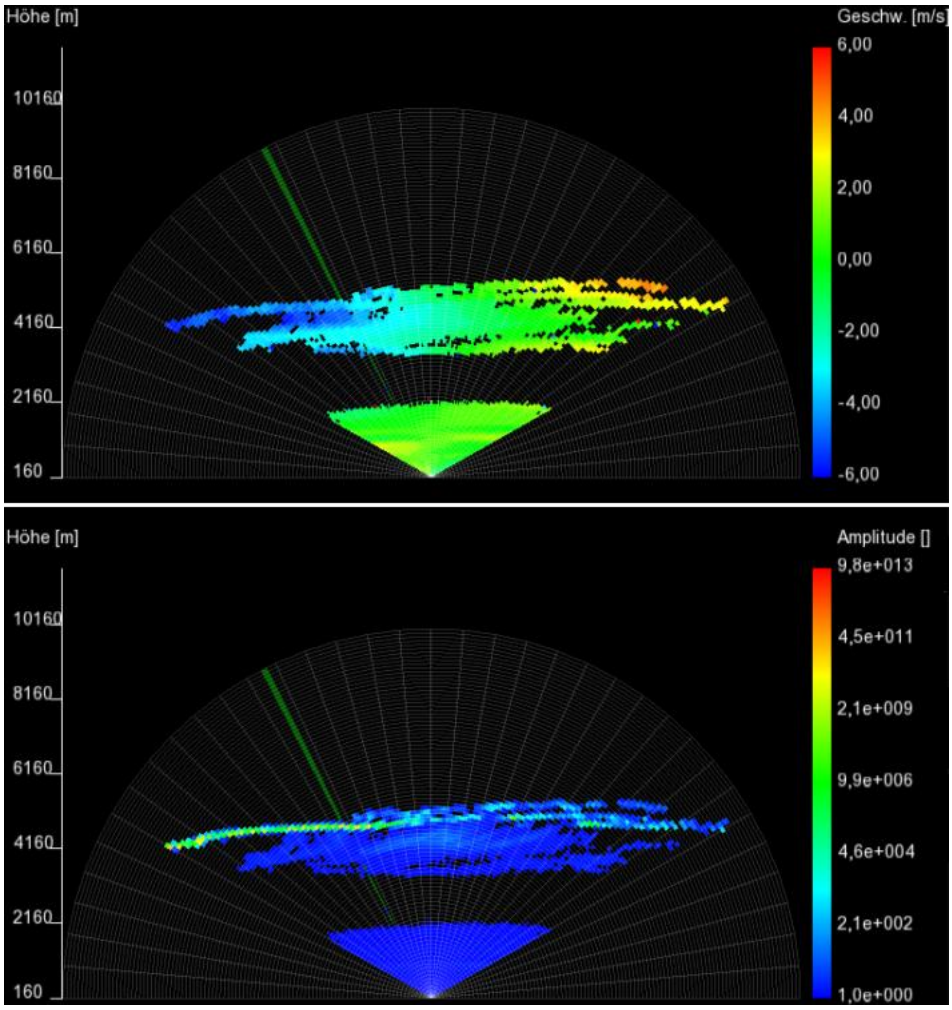

Figure 4.1: RHI atmospheric measurement recorded on the 12th of August 2015 (Top: radial wind velocity, Bottom: backscattered signal amplitude).

In the case of a long-term measurement, the elevation angle is on a fixed position. In the following measurement example in Figure 4.2 a result of such a long-term measurement is presented. This measurement was taken with an elevation angle of 10° in south direction. The range resolution according to the chosen pulse duration of 800 ns was 120 m. The peak power was SBS limited at approximately 100 W with square shaped pulses. The integration time was one second with a pulse repetition frequency of 10 kHz.

The upper graph in Figure 4.2 shows the radial velocity depending on distance as a function of time. It is seen that the gusts are moving with around 5 m/s away from the lidar system. The lower graph shows the amplitude depending on distance as a function of time. The amplitude is color coded in linear scale and not range corrected. The loss-of-signal is around 5500 m. Under those atmospheric conditions the lidar measures up to 50 range gates in average. Between 15:00 and 15:20, as well as at 15:40, clouds were measured at a distance of 5000 m, shown by a very strong backscattered signal.

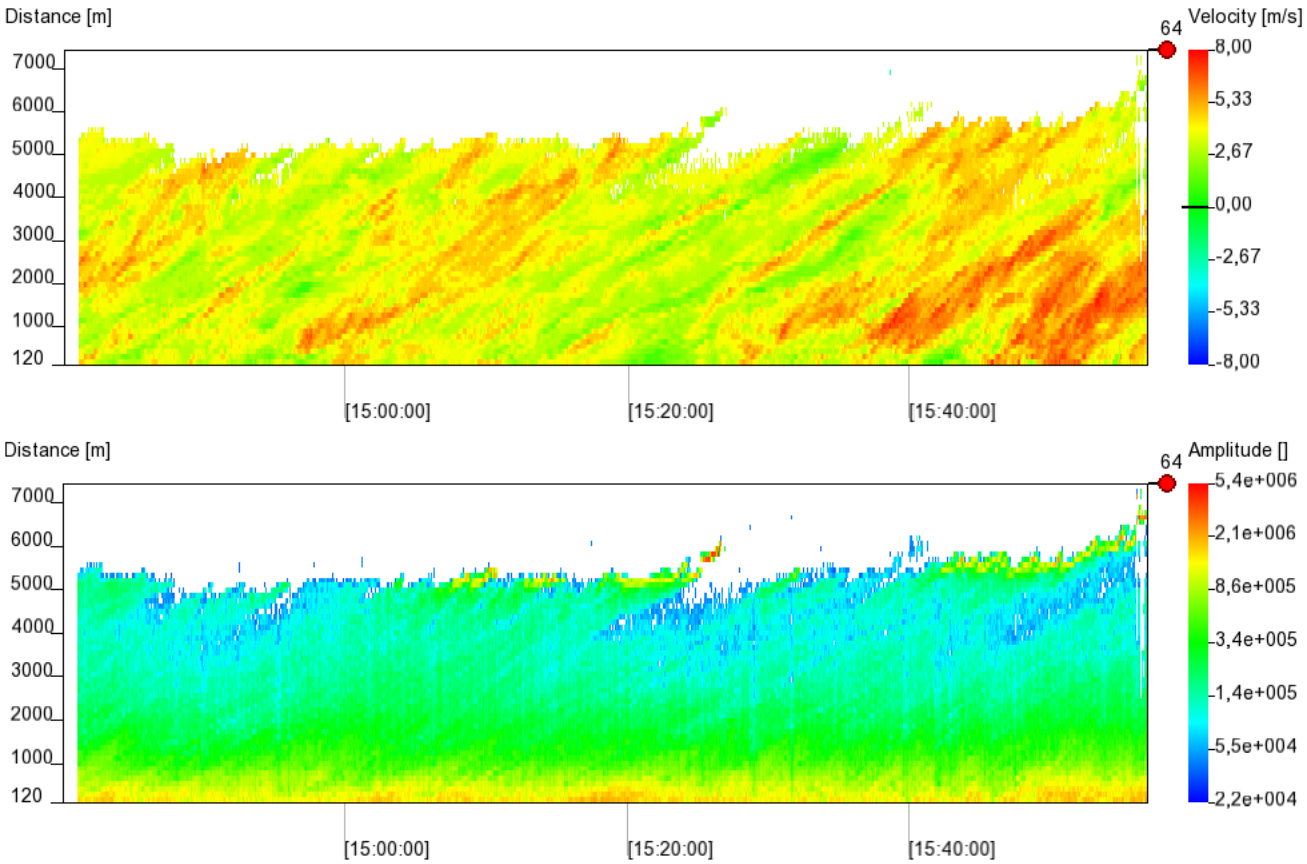

Figure 4.2: Long-term measurement recorded on the 11th of August 2015 (Top: radial wind velocity, Bottom: Backscattered signal amplitude).

5. CONCLUSION

In conclusion we demonstrated compact monolithic wind Doppler LIDAR with a high power amplifier based on double-clad Er-doped (Yb-free) fiber amplifier. It is shown that significant factor that limits the maximum peak power is the SBS threshold in the output passive components. An all-fiber circulator, coupler and collimator based on specially passive LMA PM fiber have been developed. The pulse peak power of 100 W was achieved in the designed amplifier, which is an order of magnitude higher compared to standard telecom-grade fiber amplifiers. This system allowed us to achieve threefold increase of the measurement range, which has become as high as 5000 m.

6. ACKNOWLEDGEMENTS

This work was supported in part by grant 15-38-20923 of the Russian Foundation for Basic Research (RFBR) and in part by the German Federal Ministry of Education and Research (BMBF) under FKZ 17055X10.

REFERENCES

[1] Töws, A. and Kurtz, A. "A multiwavelength lidar system based on an erbium-doped fiber MOPA-system," Proc. SPIE 9246, 92460T (2014).

[2] Kameyama S., Ando T., Asaka K., Hirano Y. and Wadaka S., "Compact all-fiber pulsed coherent Doppler lidar system for wind sensing," Appl. Opt., 46, pp. 1953-1962 (2007).

[3] Dilley C. E., Stephen M. A., and Savage-Leuchs M. P., "High SBS-threshold, narrowband, erbium codoped with ytterbium fiber amplifier pulses frequency-doubled to 770 nm," Opt. Express 15, 14389-14395 (2007).

[4] Codemard C., Farrell C., Dupriez P., Philippov V., Sahu J. K. and Nilsson J.," Millijoule, high-peak power, narrow-linewidth, sub-hundred nanosecond pulsed fibre Master-Oscillator Power-Amplifier at 1.55 μm," Comptes Rendus Physique 7, 170 (2006).

[5] Kotov, L. V., Likhachev, M.E., Bubnov, M. M., Paramonov, V. M., Belovolov, M.I., Lipatov, D. S. and Guryanov, A. N., "Record-peak-power all-fiber single-frequency 1550 nm laser," Laser Phys. Lett. 11, 095102 (2014).

[6] Canat, G., Renard, W., Robin, T., Cadier, B., Gouët, J. L., Lombard, L., Durecu, A. and Bourdon, P., "High peak power single frequency amplifiers based on efficient Erbium-Ytterbium doped LMA fibers," European Conference on Lasers and Electro-Optics - European Quantum Electronics Conference, CJ_12_5 (2015).

[7] Kotov, L., Likhachev, M., Bubnov, M., Medvedkov, O., Lipatov, D., Guryanov, A., Zaytsev, K., Jossent, M. and Février, S., "Millijoule pulse energy 100-nanosecond Er-doped fiber laser," Opt. Lett. 40, 1189-1192 (2015)